The Influence of Boundary Conditions on Midlatitude Jet Separation in Ocean Numerical Models

ERIC P. CHASSIGNET

Rosenstiel School of Marine and Atmospheric Science, University of Miami, Miami, Florida

PETER R. GENT

National Center for Atmospheric Research, Boulder, Colorado

(Manuscript received 28 January 1991, in final form 9 April 1991)

ABSTRACT

The separation point of a midlatitude jet from the western boundary in ocean numerical models depends upon both the governing equations and the vertical coordinate used. Systematic differences in the point of separation between level and layer models are shown. In level models, the separation usually occurs poleward of the zero wind-stress curl line, whereas, in layer models, it usually occurs equatorward. These differences are caused by two aspects of the numerical implementation. First, the wind forcing is usually assumed to act as a body force over the upper layer or level in the models, and this corresponds to a different physical assumption. Second, the free-slip boundary condition is imposed as zero vorticity in both models. This is an inconsistency because vorticity is not the same quantity when the governing equations are formulated in physical (level model) and isopycnal (layer model) coordinates. The effects on separation of these numerical implementation differences are illustrated using analytical solutions of linear models and numerical solutions of several nonlinear models.

1. Introduction

The separation issue of a midlatitude jet from the western boundary is an important question in ocean modeling, not yet fully resolved, since most existing realistic eddy-resolving North Atlantic simulations exhibit an overshooting Gulf Stream at Cape Hatteras [see Thompson and Schmitz (1989) for a review]. At the present time, increasing activity in the study of the earth's climate demands validated ocean circulation numerical models, and it is therefore important to carefully explore and explain the limitations and implications of each model choice. When comparing several adiabatic wind-driven, eddy-resolving numerical models of idealized midlatitude basins, it is noticeable that the point of separation varies quite widely depending upon both the governing equations and the vertical coordinate used. Models using levels or physical coordinates have separation in a different location than those using a stack of isopycnal layers. Pedlosky (1979) discusses the justification for layer models and concludes, "While the finite-level models are gross mathematical approximations to an accurate portrayal of the true physical systems, the layer models invert this relationship and serve as accurate mathematical representations of a crude physical representation of actually more complex geophysical systems." The layer model equations can also be justified as a finite difference approximation to the continuous equations transformed to isopycnal coordinates.

Two differences between the formulation of level and layer numerical models are immediately apparent. Usually the wind forcing is assumed to act as a body force over the upper level or layer in the models, and it is shown that this different physical assumption has a considerable influence upon the point of separation. Lateral dissipation is also different in the models because it acts along levels or along isopycnals. In fact, one reason to prefer layer models is that mixing of material properties by eddies in the ocean is thought to occur primarily along isopycnals. We have no evidence that lateral dissipation acting along levels or isopycnals influences the point of separation, but the coefficient and form of the lateral dissipation certainly do. The reason is that the point of separation depends on how inertial the western boundary current is. However, with dissipation, viscous boundary conditions must be specified. With Laplacian friction, the no-slip boundary condition of zero tangential velocity is identical in physical and isopycnal coordinates. However, the free-slip boundary condition has been imposed as zero vorticity in both level and layer models. This is a difference in model physics because vorticity in physical and isopycnal coordinates is not the same quantity. This distinction in the physical significance of the free-slip boundary condition between models is shown to have

Corresponding author address: Dr. Eric P. Chassignet, University of Miami, RSMAS/MPO, 4600 Rickenbacker Causeway, Miami, FL 33149-1098.

an influence upon the point of separation. If biharmonic friction is used, and additional, higher-order, boundary conditions are required, then the level and layer models' responses will be inconsistent for both no-slip and free-slip boundary conditions since the usual quantities set to zero are not the same in physical and isopycnal coordinates. The reader is referred to Holland (1978) for a discussion on the use of the two types of friction (Laplacian or biharmonic) in ocean numerical models.

The layout is the following. In section 2, the models' characteristics and parameters are first reviewed and, then, their mean responses are described and compared. Section 3 investigates the influence of the prescribed boundary conditions, namely, wind forcing at the upper surface and zero vorticity at the walls. The results are then discussed and summarized in the concluding section.

2. The numerical models

a. Description and parameters

The four numerical models that are considered in this comparison are quasi-geostrophic in physical coordinates (QG) (Holland 1978; McWilliams et al. 1990), linear balance equations in physical coordinates (LBE) (McWilliams et al. 1990), primitive equations using a stack of isopycnal layers (Bleck and Boudra 1986, here after BB), and primitive equations in sigma coordinates (SPEM)[1] (Haidvogel et al. 1991). They are all configured in a rectangular ocean basin (3600 km $\times$ 2800 km $\times$ 5 km) driven by a zonally symmetric wind stress $\vec{\tau} = [-\tau_m \cos(2\pi y/L), 0]$, where $\tau_m = 1 \times 10^{-4}$ m^2 s^{-2}, and damped by both a lateral eddy viscosity of the biharmonic form ($A_4 = 8 \times 10^{10}$ m^4 s^{-1}) and a linear bottom drag ($\nu = 3.3 \times 10^{-7}$ s^{-1}). The lateral boundary conditions employed on the four sidewalls are free slip. In both horizontal coordinates, the grid is uniform with a spacing of 20 km. In the vertical, the spacing (four levels or layers) is nonuniform, with greater resolution near the upper surface. The initial stratification, which corresponds to a first baroclinic deformation radius of 44.7 km, is defined as

$$N^2(z) = -\frac{g}{\rho_o}\frac{\partial \rho}{\partial z} = 5.9 \times 10^{-5} \exp(z/800)$$

where N^2 is in s^{-2} and z in meters. The resulting circulation is nearly antisymmetric about midlatitude with a counterclockwise gyre north of the wind-stress curl and a clockwise gyre to the south.

The QG and LBE models are z-coordinates in the vertical, and as such, the variables are located on two sets of vertical grid points,[2] defined as levels (McWilliams et al. 1990). On the other hand, SPEM uses a stretched vertical coordinate system that conforms to the variable bottom. Such "sigma" coordinates are equivalent to z coordinates when a flat bottom is prescribed. A semispectral method (Haidvogel et al. 1991) has been implemented to solve the vertical structure[3] versus the centered, second-order finite-difference scheme of QG and LBE (McWilliams et al. 1990). The BB model is a stack of shallow fluid layers,[4] each one characterized by a constant value of density. The motion within each layer is governed by a momentum and a continuity equation. The layers interact through hydrostatically transmitted pressure forces. Vorticity and horizontal velocities are defined as mean layer properties. Pressure and geopotential are defined at the interfaces between layers. For more details on the implementation of each numerical model, the reader is referred to Bleck and Boudra (1986), McWilliams et al. (1990), and Haidvogel et al. (1991), respectively.

b. Mean flow pattern and midlatitude jet separation location

The time average of the upper streamfunction for the four numerical models are presented in Fig. 1. The QG model differs from its counterparts by its symmetric mean response about the middle latitude of the basin. The approximations made to obtain the quasi-geostrophic equations and boundary conditions imply a symmetric response when a symmetric forcing is specified. As soon as the latter is relaxed, the midlatitude jet exhibits asymmetries (Verron and Le Provost 1989). The mean path of the midlatitude jet in the other models does exhibit a standing wave pattern whose amplitude decays into the interior. The midlatitude jet is also characterized by a reduced strength and a reduced penetration into the interior. Both LBE and SPEM show a northward location of the separation point when compared to QG. In BB, on the contrary, the mean position of the separation point is located *south* of the zero wind-stress curl line (ZWCL). The stratification is such that the upper level did not outcrop anywhere in the basin.

In order to quantify the differences in the separation point location, time series of its location are presented in Fig. 2 for the different models. As expected, the QG mean separation point is located at the ZWCL and the fluctuations are confined within a small band of 200-km width. The LBE model has a mean separation point located 100 km north of the ZWCL and has greater fluctuations (plus or minus 200 km). SPEM does not separate as far north (75 km) and has less variability. As stated previously, the mean separation point in BB is significantly south of the ZWCL (105 km) and its

[1] Semispectral Primitive Equation Model.

[2] [0, −440, −1048, −2016, −5000] and [−208, −712, −1456, −2896], respectively (in meters).

[3] [0, −216, −1030, −2761, −5000] for the collocation points (in meters).

[4] [440, 608, 978, 2974] for the mean layer thicknesses (in meters).

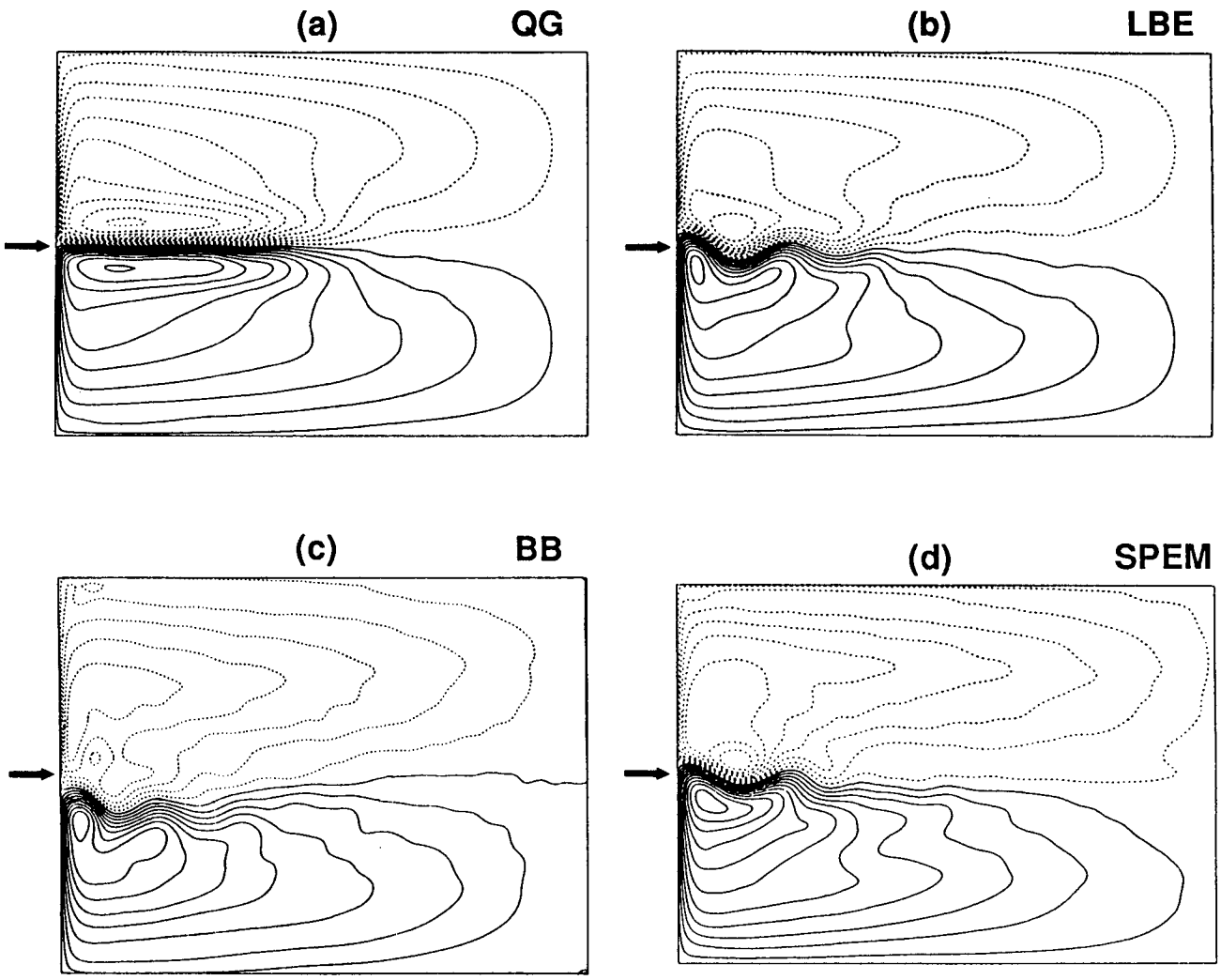

FIG. 1. Time average of the upper nondivergent streamfunction for the following numerical models: (a) quasi-geostrophic (QG) (40-year average), (b) linear balance (LBE) (40-year average), (c) primitive equation isopycnal coordinates (BB) (10-year average), and (d) primitive-equation sigma coordinates (SPEM) (7-year average). The contour intervals are 10^4 m^2 s^{-1} and the contour values straddle zero symmetrically. The arrow points to the zero wind-stress curl line (ZWCL).

position fluctuates greatly (up to 300 km) which explains the broader jet in Fig. 1c. Table 1 summarizes the characteristics of the separation point for the four numerical models.

The linear balance equations (Lorenz 1960) are an improvement over quasi geostrophy by relaxing the β-plane form of the Coriolis force and the linearization of the buoyancy equation about a steady, horizontally uniform density stratification. McWilliams et al. (1990) found in LBE a subtropical gyre much more surface intensified than in QG. Their explanation in terms of vorticity is that the horizontal fluxes (primarily advective) are mainly balanced by the vortex stretching term fw_z. If the horizontal fluxes are equal between the gyres, fw_z is equal. In QG, the stretching term is $f_o w_z$ and no gyre asymmetry results. In LBE, since f is smaller in the south, w_z is larger and the resulting circulation is more surface intensified. It is then reasonable to assume that a stronger surface western boundary current in the south moves the separation point north of the ZWCL. This is the case for LBE when free-slip boundary conditions are adopted.[5] This explanation also applies to the primitive equations and the question then arises as to why the BB primitive equation model behaves differently.

c. *Jet separation in layer models*

The early separation of the midlatitude jet observed in the BB model was first pointed out by Bleck and

[5] One expects the model's response to be dependent upon the choice of the lateral boundary conditions (Moro 1988).

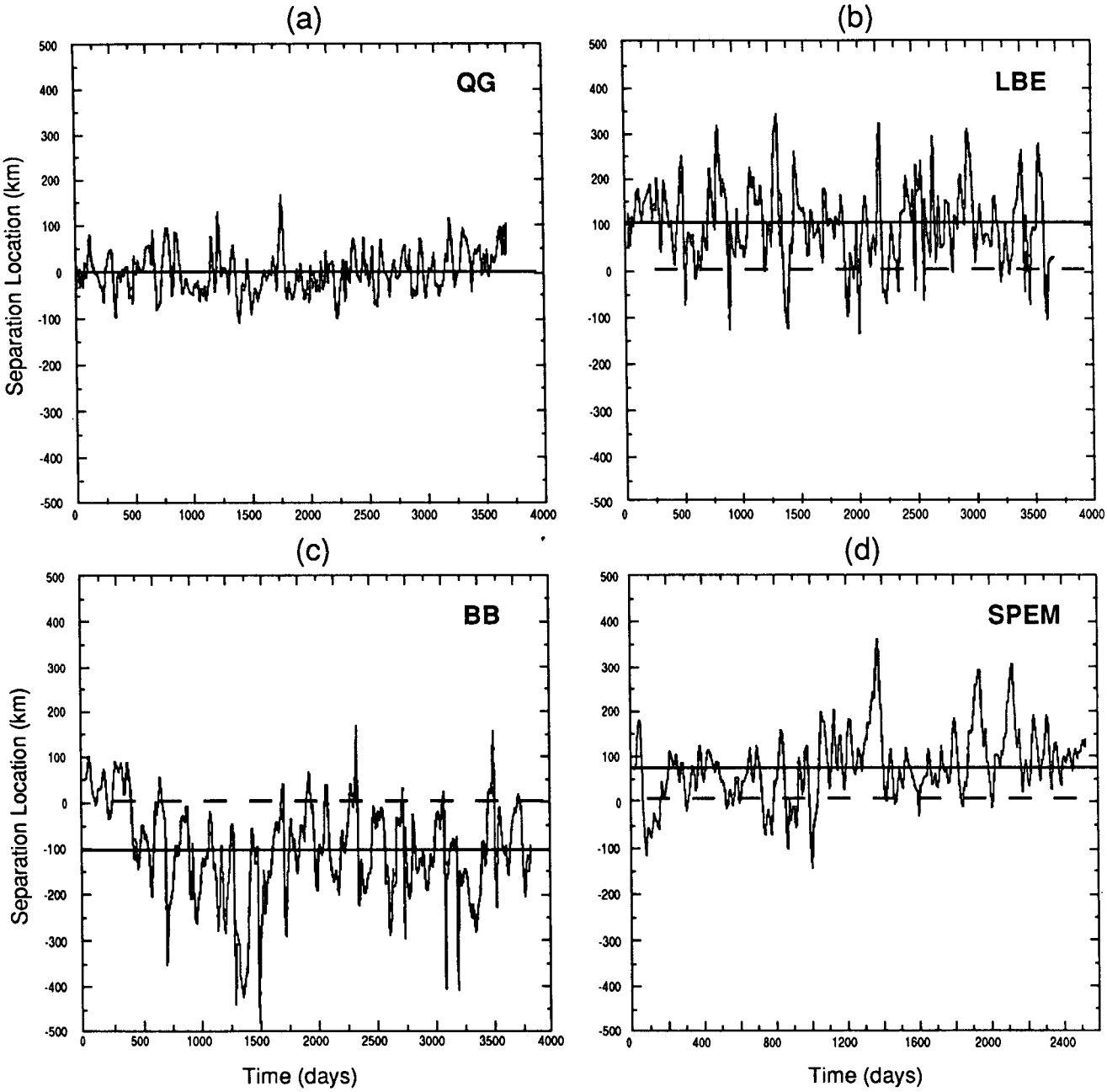

FIG. 2. Time series of the midlatitude jet separation location as a deviation from the ZWCL (in kilometers) for the following numerical models: (a) quasi-geostrophic (QG), (b) linear balance (LBE), (c) primitive-equation isopycnal coordinates (BB), and (d) primitive-equation sigma coordinates (SPEM).

Boudra (1981, 1986) in a comparison of the model's behavior with the stacked layer model of Holland and Lin (1975). They showed that, for the same basin configuration, except with four layers instead of two, their mean gyre patterns were considerably less symmetric with respect to the wind forcing and that the asymmetry resulted from a pronounced southward shift of the separation point of the free jet relative to the position of the maximum wind stress. They suggested that the enhanced vertical resolution in the upper 1000 m in BB, thought to be of considerable importance in the development of the gyre-scale circulation, was responsible for the different patterns. However, the experiments presented in Fig. 1 for QG, LBE, and SPEM have a similar vertical resolution as Bleck and Boudra (1981, 1986), but as stated earlier, do not show this tendency

TABLE 1. Characteristics of the midlatitude jet separation location as a deviation from the ZWCL for QG, LBE, BB, and SPEM.

Numerical model	Mean deviation from ZWCL (km)	Root-mean-square displacement of the separation point (km)
QG	1.2	46.2
LBE	101.4	88.0
BB	−103.6	108.5
SPEM	77.1	77.8

for the jet to separate south of the ZWCL. This strongly suggests that the differences in the location of the separation point are not due to the lack of vertical resolution as first suggested by the comparison with Holland and Lin (1975).

At this point, one would like to assess whether the early separation observed in BB is characteristic of layer models of higher vertical resolution. In order to answer this question, the BB model's response was compared to the Holland and Lin (1975) model[6] (HL) when configured in the same domain (i.e., 2000 × 2000 × 5 km) and with three layers (400, 800, and 3800 m, respectively). Both models are discretized in the vertical by a stack of layers of constant density, each governed by the shallow-water equations. The lateral eddy viscosity is of the Laplacian form with $A_M = 300$ m^2 s^{-1} and the boundary conditions on the sidewalls are free slip. The reader is referred to Holland and Lin (1975) and Bleck and Boudra (1981, 1986) for more details. The time average of the first interface depth is presented in Fig. 3 for the two numerical models and it shows that the flow patterns are very similar and exhibit a midlatitude jet that separates south of the zero wind-stress curl line. We attribute the fact that the flow patterns are not identical to the different numerical formulations and different lengths of the time averages. Thus, we conclude that the early separation is characteristic of layer models. This is consistent with Huang's (1986) study of the wind-driven circulation of a subtropical/subpolar basin with a linear shallow-water numerical model. He observed highly asymmetric circulation patterns for a symmetric wind forcing with a midlatitude jet south of the ZWCL. The question then arises as to which properties of the layer model formulation are responsible for this behavior.

3. Influence of the boundary conditions

In this section, we investigate the influence on the midlatitude jet separation of, first, the wind-forcing prescription at the ocean surface and, second, of the lateral boundary conditions at the walls.

[6] Courtesy of K. Haines and W. Holland.

a. *The wind-forcing prescription and its impact on the interior solution*

For all numerical models, the wind stress is applied as a body force, at the uppermost level for QG, LBE, and SPEM and over the uppermost layer in BB and HL. A simple study of the interior solution for both coordinate systems (level and layer) will illustrate the importance of this wind-forcing prescription. As for the experiments described in section 2, the wind stress is zonally symmetric of the form $\vec{\tau} = [\tau, 0]$ with $\tau = -\tau_m \cos(2\pi y/L)$.

Consider the two-level (layer) system. For the directly wind-driven circulation (uppermost level or layer), the upper u-momentum equation in the absence of dissipation for the level model is expressed as

$$\frac{Du}{Dt} - fv = -\frac{1}{\rho}\frac{\partial p}{\partial x} + \frac{\tau}{H_1} \tag{1}$$

while for the layer model of comparable stratification, it is expressed as

$$\frac{Du}{Dt} - fv = -\frac{1}{\rho}\frac{\partial p}{\partial x} + \frac{\tau}{h} \tag{2}$$

where h is the upper-layer thickness ($H_1 + h'$). In the layer model, the acceleration then depends on the upper-layer thickness, stronger in the northern cyclonic cell (negative h') and weaker in the southern anticyclonic cell (positive h') (Fig. 3).

The importance of the difference in the above formulation is illustrated through an analysis of the vorticity equation for both systems. The conservation of the relative vorticity $\zeta = \partial v/\partial x - \partial u/\partial y$ for a primitive equation fluid in the absence of dissipation is

$$\frac{\partial \zeta}{\partial t} + \mathbf{u}\cdot\nabla\zeta - (\zeta + f)\frac{\partial w}{\partial z} + \beta v = F \tag{3}$$

where $\mathbf{u} = (u, v, w)$ and F represents any vorticity forcing function.

Under the assumption of quasi-geostrophic dynamics, several terms drop out of (3), the horizontal velocity can be defined in terms of a streamfunction, and the simplified equation for the upper level is

$$\frac{D}{Dt}(\nabla^2\psi_1 + f) - \frac{f_o}{H_1}\frac{Dh'}{Dt} = \frac{\mathrm{curl}_z\vec{\tau}}{H_1} \tag{4}$$

where $h' = f_o(\psi_1 - \psi_2)/g'$ is the deviation of the interface height from its equilibrium position and ψ_i, the streamfunction at level i (Holland 1978). At this point, for simplicity, we assume a steady flow, a motionless lower layer, and we neglect the inertial terms. Equation (4) then reduces to

$$\beta\frac{\partial \psi_1}{\partial x} = \frac{\mathrm{curl}_z\vec{\tau}}{H_1} \tag{5}$$

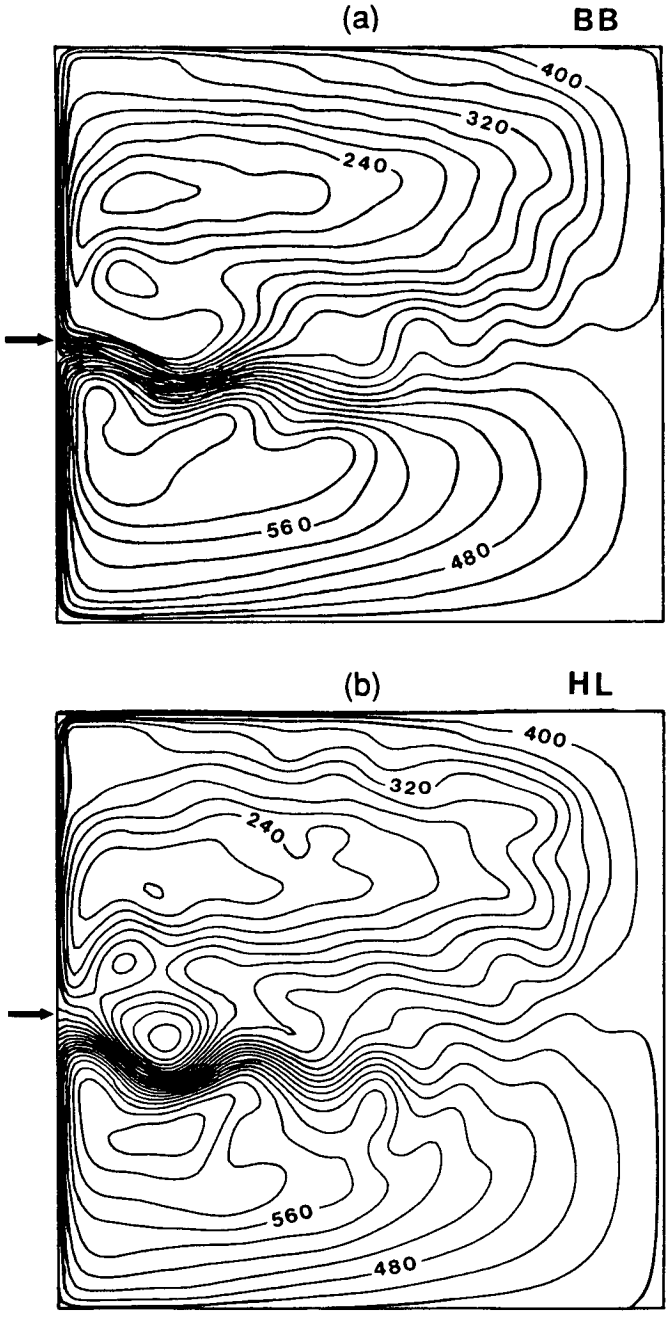

FIG. 3. Time average of the upper-layer thickness for the following numerical models (in meters): (a) Bleck and Boudra (1986) (BB) (5-year average) and (b) Holland and Lin (1975) (HL) (1-year average). Both use a Laplacian eddy viscosity of $A_M = 300\ \mathrm{m^2\ s^{-1}}$.

and the steady solution for the interior flow, which satisfies the boundary condition of $\psi_1 = 0$ at the eastern boundary, is the Sverdrup solution

$$\psi_1 = \frac{(L-x)}{\beta H_1}\frac{\partial \tau}{\partial y}. \tag{6}$$

The corresponding velocities $u = -\partial\psi_1/\partial y$, $v = \partial\psi_1/\partial x$ are defined as

$$u = -\frac{(L-x)}{\beta H_1}\frac{\partial^2 \tau}{\partial y^2}, \quad v = -\frac{1}{\beta H_1}\frac{\partial \tau}{\partial y}. \tag{7}$$

This solution is symmetric with respect to the zero wind-stress curl line (ZWCL). For this quasi-geostrophic steady flow, vortex stretching due to the interface displacement is absent and the solution is equivalent to the barotropic solution.

McWilliams et al. (1990) inferred that the correction to the Coriolis frequency in LBE is dynamically more important than the divergent buoyancy advection. They showed that the LBE results were close to those from an intermediate model (gQG), which keeps the geostrophic buoyancy balance of QG, but possesses the general form of the Coriolis force. The vorticity equation for such a model can be derived from (3) and is

$$\frac{D}{Dt}(\nabla^2\psi_1 + f) - \frac{f}{H_1}\frac{Dh'}{Dt} = \frac{\mathrm{curl}_z\vec{\tau}}{H_1} \tag{8}$$

with $h' = f(\psi_1 - \psi_2)/g'$. Again, we consider a motionless lower layer and we neglect the inertial term. The steady interior streamfunction must then obey

$$\beta\frac{\partial \psi_1}{\partial x} - \frac{f\beta}{2g'H_1}\frac{\partial {\psi_1}^2}{\partial x} = \frac{\mathrm{curl}_z\vec{\tau}}{H_1} \tag{9}$$

and a solution that satisfies the boundary condition $\psi_1 = 0$ at the eastern boundary is

$$\psi_1 = \frac{g'H_1}{f}\left[1 - \left(1 - \frac{2f}{g'{H_1}^2}\frac{(L-x)\partial\tau/\partial y}{\beta}\right)^{1/2}\right] \tag{10}$$

or to first order,

$$\psi_1 = \frac{(L-x)}{\beta H_1}\frac{\partial \tau}{\partial y}\left(1 + \frac{1}{2}\frac{f_o(L-x)\partial\tau/\partial y}{\beta g'{H_1}^2} + \cdots\right). \tag{11}$$

The corresponding velocities are defined as

$$u = -\frac{(L-x)}{\beta H_1}\frac{\partial^2 \tau}{\partial y^2}\left(1 + \frac{f_o(L-x)\partial\tau/\partial y}{\beta g'{H_1}^2} + \cdots\right), \tag{12}$$

$$v = \frac{-1}{\beta H_1}\frac{\partial \tau}{\partial y}\left(1 + \frac{f_o(L-x)\partial\tau/\partial y}{\beta g'{H_1}^2} + \cdots\right). \tag{13}$$

This solution is asymmetric with respect to the ZWCL with a stronger circulation in the subtropical gyre and weaker in the subpolar gyre. This is consistent with the findings of McWilliams et al. (1990) since this suggests a northward shift in the separation point when nonlinearity and inertial effects are included.

The layer model differs from its level counterpart by the formulation of its forcing, which is dependent on the upper-layer thickness. To illustrate the importance of the latter, we now consider another intermediate

model, namely, QG with a forcing dependent on $H_1 + h'$. The vorticity equation is

$$\frac{D}{Dt}(\nabla^2\psi_1 + f) - \frac{f_o}{H_1}\frac{Dh'}{Dt} = \frac{\text{curl}_z\vec{\tau}}{H_1 + h'} \tag{14}$$

with $h' = f_o(\psi_1 - \psi_2)/g'$. The steady interior streamfunction with the same approximations as previously will then obey

$$\beta\frac{\partial\psi_1}{\partial x} + \frac{f_o\beta}{2g'H_1}\frac{\partial\psi_1^2}{\partial x} = \frac{\text{curl}_z\vec{\tau}}{H_1}. \tag{15}$$

A first-order solution that satisfies the boundary condition $\psi_1 = 0$ at the eastern boundary is

$$\psi_1 = \frac{(L-x)}{\beta H_1}\frac{\partial\tau}{\partial y}\left(1 - \frac{1}{2}\frac{f_o(L-x)\partial\tau/\partial y}{\beta g'H_1^2} + \cdots\right) \tag{16}$$

and the corresponding velocities are defined as

$$u = -\frac{(L-x)}{\beta H_1}\frac{\partial^2\tau}{\partial y^2}\left(1 - \frac{f_o(L-x)\partial\tau/\partial y}{\beta g'H_1^2} + \cdots\right), \tag{17}$$

$$v = \frac{-1}{\beta H_1}\frac{\partial\tau}{\partial y}\left(1 - \frac{f_o(L-x)\partial\tau/\partial y}{\beta g'H_1^2} + \cdots\right). \tag{18}$$

Again, this solution is asymmetric with respect to the ZWCL, but this time with a stronger circulation in the subpolar gyre and weaker in the subtropical gyre. This suggests a southward shift of the separation point in a nonlinear model and is consistent with the primitive-equation layer model given below.

The upper-layer momentum equations for the primitive equations with the same approximations as before are those of the reduced-gravity model

$$-fv = -g'\frac{\partial h}{\partial x} + \frac{\tau}{h}, \quad fu = -g'\frac{\partial h}{\partial y}. \tag{19}$$

The solution for the interior is then expressed as

$$u = -\frac{(L-x)}{\beta h}\frac{\partial^2\tau}{\partial y^2}, \quad v = -\frac{1}{\beta h}\frac{\partial\tau}{\partial y} \tag{20}$$

with the upper-layer thickness h defined as

$$h = \left[h_e^2 + \frac{2(L-x)}{g'}\left(\frac{f}{\beta}\frac{\partial\tau}{\partial y} - \tau\right)\right]^{1/2} \tag{21}$$

where h_e is the layer thickness at the eastern boundary (Welander 1966; Parsons 1969; Huang and Flierl 1987). The derived height field h is asymmetric with respect to the ZWCL, is strongly dependent on the choice of τ_m and H_1, and is shallower in the subpolar gyre and deeper in the subtropical gyre (Fig. 4) (Huang 1986). The resulting circulation is clearly not symmetric with respect to the ZWCL with stronger flows in the subpolar gyre and weaker flows in the subtropical gyre. The tendency for northward separation due to the full Coriolis force is then overcome by the tendency for southward separation due to the effect of the wind-forcing formulation.

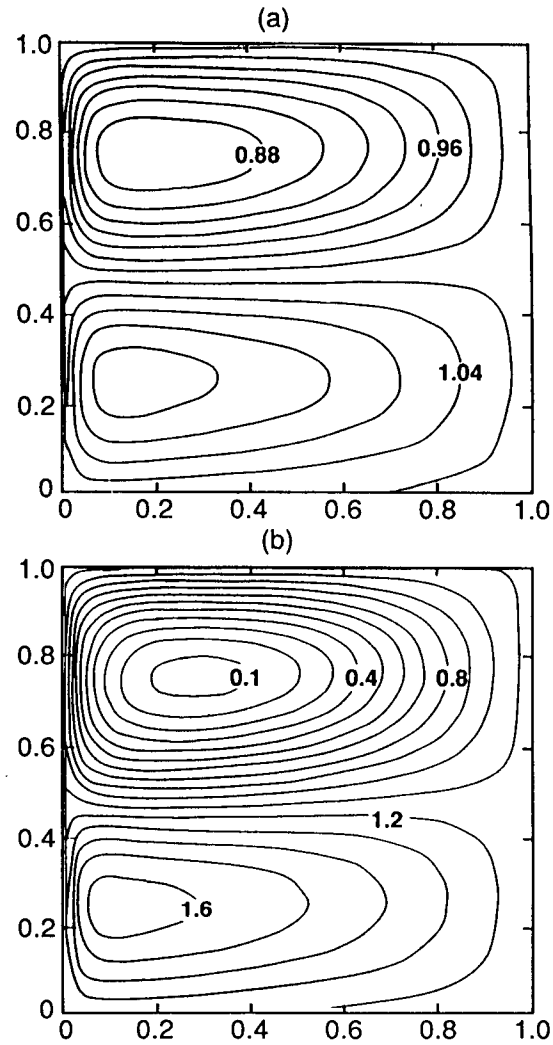

FIG. 4. Nondimensional isobaths as a function of $\lambda = L\tau_m/g'H_1^2$. (a) $\lambda = 0.0333$. Slight departure from symmetry; (b) $\lambda = 0.2$. The upper layer barely covers the entire basin and the flow pattern is asymmetric. After Huang (1986).

In summary, steady noninertial solutions in the absence of dissipation differ substantially depending on the choice of the vertical coordinate and the corresponding wind-forcing formulation. In all the above linear solutions, no particles cross the ZWCL (v is identically equal to zero for $y = L/2$) and one expects the solutions to be significantly altered once inertia, time dependence, and dissipation are included. It is reasonable to assume that a northward overshooting of the midlatitude jet will occur for cases with surface intensified subtropical gyres (level models) and southward for cases with surface intensified subpolar gyres (layer models).

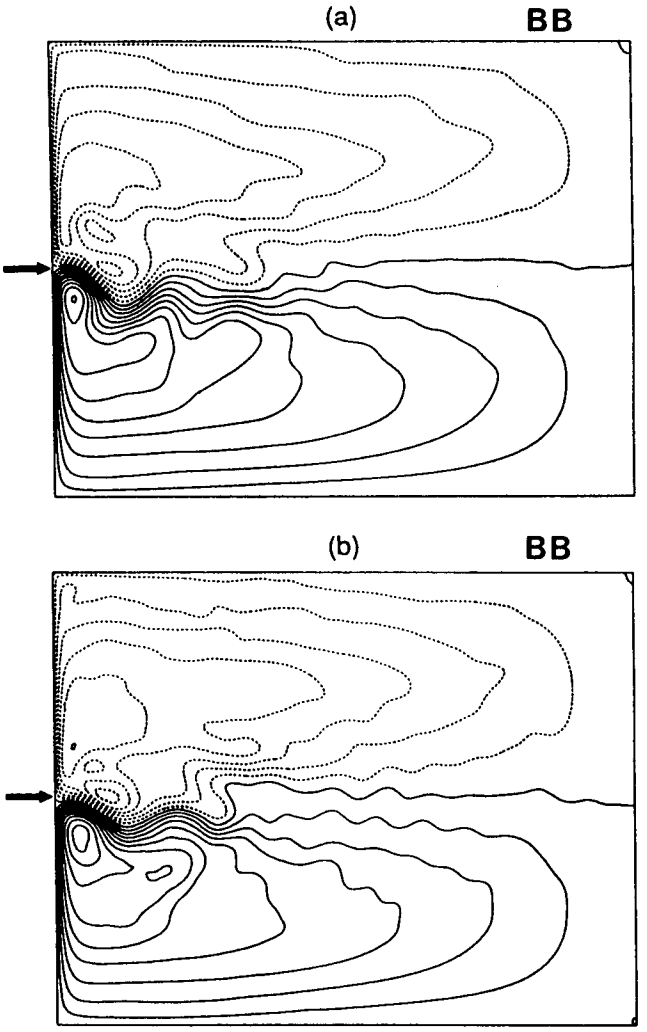

FIG. 5. Five-year time average of the upper-layer nondivergent streamfunction for the isopycnal coordinate primitive-equation numerical model (BB) with a Laplacian eddy viscosity: (a) $A_M = 200$ m^2 s^{-1} and (b) $A_M = 100$ m^2 s^{-1}. Contour intervals and values as in Fig. 1.

b. *Boundary condition at the walls*

The separation results described in section 2b were for models using a biharmonic friction. Viscous wall boundary conditions are much simpler to implement and interpret in numerical models when the horizontal mixing is of the Laplacian form. Thus, in this section, the importance of the boundary conditions at the wall on the separation issue is explored with numerical models using Laplacian friction. With symmetric lateral boundary conditions, this change does not break the symmetry properties in QG, so that the mean separation point will still be at the ZWCL. The primitive-equation layer model of BB using Laplacian friction has been run with $A_M = 200$ and 100 m^2 s^{-1}, respectively. The latter value more closely matches the values of biharmonic friction used in section 2b, but the changed boundary condition formulation described below is only stable using the larger value. The time-averaged streamfunctions in the upper layer for these two cases are shown in Fig. 5. When a value of 200 m^2 s^{-1} is used for the Laplacian operator, the midlatitude jet separation latitude is shifted to approximately the ZWCL (Fig. 5a). This is considerably farther north than in the BB model with biharmonic friction (Fig. 1c). However, the separation point is still significantly farther south than in LBE and SPEM with biharmonic friction. This is consistent with the decrease in inertia induced by the change in dissipation. When inertia is increased ($A_M = 100$ m^2 s^{-1}), the latitude of separation is shifted south by 40 km (Fig. 5b). This case resembles the more inertial biharmonic friction case shown in Fig. 1c.

The two most common viscous boundary conditions used in ocean numerical models are either free slip (zero vorticity at the wall) or no slip (zero tangential velocity at the wall). The free-slip boundary condition, used in the experiments presented in section 2, requires the vorticity ($\zeta = \partial v/\partial x - \partial u/\partial y$) to be equal to zero on the boundary. In level models, the derivatives are computed on surfaces of constant depth while for layer models, they are computed on surfaces of constant density (isopycnal surfaces).

Transforming from physical or depth coordinates to isopycnal coordinates gives

$$\left(\frac{\partial}{\partial x}\right)_z = \left(\frac{\partial}{\partial x}\right)_\alpha - \left(\frac{\partial z}{\partial x}\right)_\alpha \frac{\partial}{\partial z} \tag{22}$$

where $\alpha = \rho^{-1}$. Vorticity in isopycnal coordinates, ζ_α, is related to vorticity in z-coordinates, ζ_z, by

$$\zeta_\alpha = \zeta_z + \left(\frac{\partial z}{\partial x}\right)_\alpha \frac{\partial v}{\partial z} - \left(\frac{\partial z}{\partial y}\right)_\alpha \frac{\partial u}{\partial z}. \tag{23}$$

Thus, setting the vorticity to zero at the wall in one coordinate system does not imply the same condition in the other reference frame ($\zeta_z = 0$ is not equivalent to $\zeta_\alpha = 0$ and vice versa). In the isopycnal framework, following the notation of Bleck and Boudra (1986), (23) can be rewritten using the geostrophic approximation as

$$\zeta_\alpha = \zeta_z + \frac{1}{f\partial p/\partial \alpha}\left[\left(\frac{\partial p}{\partial x}\right)_\alpha^2 + \left(\frac{\partial p}{\partial y}\right)_\alpha^2\right]. \tag{24}$$

The additional term becomes important in regions of steep gradients, which are along the western boundary in the numerical experiments described above. Estimates of its magnitude are in some locations as high as 10% of the Coriolis parameter f. In QG, following the notation of McWilliams et al. (1990), relation (23)

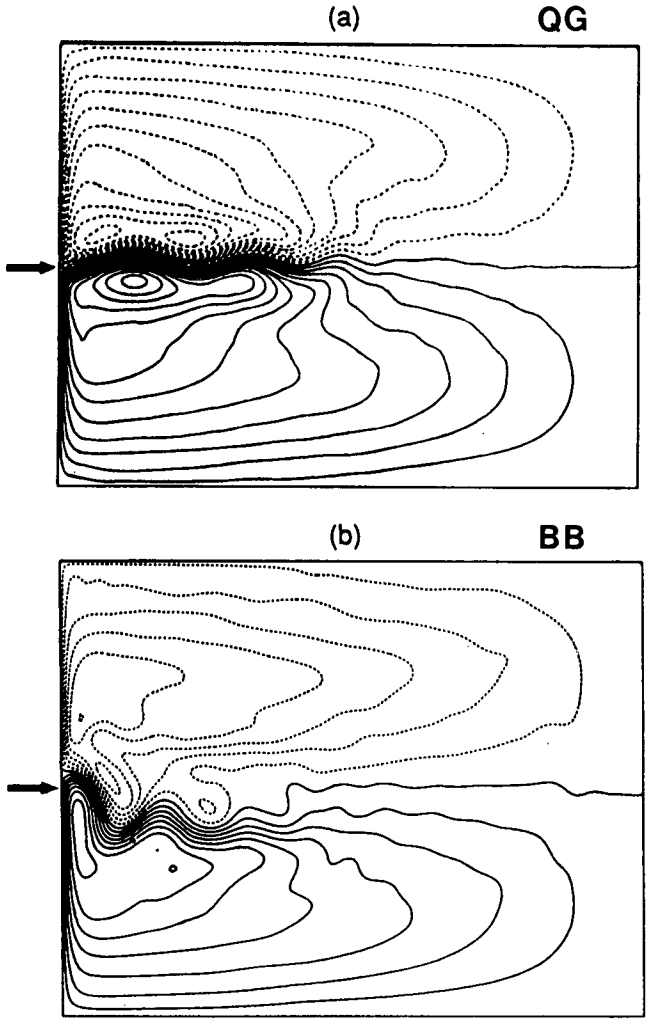

FIG. 6. Time average of the upper-nondivergent streamfunction for (a) the quasi-geostrophic (QG) numerical model with $\zeta_\alpha = 0$ (20-year average, $A_M = 80\ m^2\ s^{-1}$) and (b) the isopycnal coordinate (BB) numerical model with $\zeta_z = 0$ (5-year average, $A_M = 200\ m^2\ s^{-1}$). Contour intervals and values as in Fig. 1.

between the two expressions for the vorticity on boundaries is expressed as

$$\zeta_z = \zeta_\alpha + f_o \frac{\psi_{nz}^2}{T_z}. \tag{25}$$

In order to investigate this inconsistency, two numerical experiments were performed. The first one was with the level QG model and $\zeta_\alpha = 0$ in (25) prescribed at the walls. Note that the right-hand side term in (25) is small and would normally be omitted in QG. Retaining this term does break the symmetric properties of QG and the separation point no longer must be at the ZWCL. The second experiment was performed with the BB model and $\zeta_z = 0$ in (24) is prescribed at the walls.

The time averages of the upper-level and layer streamfunction for both numerical models with the new boundary conditions are presented in Fig. 6. Both experiments, QG and BB with the new boundary conditions, show a significant shift in the position of the midlatitude jet with respect to their previous separation latitude with the usual boundary conditions. On one hand, as shown in Fig. 6, QG with $\zeta_\alpha = 0$ exhibits a southward displacement of the jet's separation by about 30 km, while BB with $\zeta_z = 0$ displays a northward shift of the separation latitude of 80 km (compare Fig. 6b to Fig. 5a). Thus, in the free-slip case, the differences in the imposed conditions of zero vorticity at the walls contributes significantly to the difference between level and layer models in midlatitude jet separation (namely, a southern separation for layer models).

When the no-slip boundary condition is imposed, there is no difference in physical and isopycnal coordinates because the velocities are the same. If biharmonic friction is used, however, then there will be an inconsistency for both free-slip and no-slip cases if the usual higher order boundary conditions are implemented in both models.

4. Discussion and conclusions

The impact of the different wind-forcing formulation in level and layer models can be further illustrated by considering the global Rossby numbers, ϵ_N and ϵ_S, associated with the northern and southern gyres, respectively. In the level model, both are identical and equal to $\epsilon = \tau_m/(H_1\beta^2 L^3)$. In the layer model, the two Rossby numbers will differ because of the differences in mean layer thicknesses in the two gyres, stronger in the northern gyre (average layer thickness less than H_1) and weaker in the southern gyre (average layer thickness greater than H_1). The importance of such an asymmetry is illustrated by the study of the response of a QG model to asymmetric wind forcing by Verron and Le Provost (1989). They derived a statistical relationship between the latitude of the jet's detachment and the wind-forcing asymmetry. If only the relative strength of the wind stress in the two gyres is varied, then the position of the jet's detachment for an asymmetric wind in their experiments is approximated by

$$y_S = \frac{L}{2}\left(1 - \frac{\tau_m{}^N - \tau_m{}^S}{\tau_m{}^N + \tau_m{}^S}\right) \tag{26}$$

where $\tau_m{}^N$ and $\tau_m{}^S$ are the maximum wind stress associated with the northern and southern gyre, respectively. If the Rossby number is considered to be characteristic of the asymmetry, then (26) can be expressed as function of ϵ_N and ϵ_S. By further replacing the Rossby numbers by their respective expressions for the layer model, then, for a symmetric wind forcing, the separation latitude will be given by

$$y_S = \frac{L}{2}\left(1 - \frac{\bar{h}_S - \bar{h}_N}{\bar{h}_S + \bar{h}_N}\right) \quad (27)$$

where $\bar{h}_N$ and $\bar{h}_S$ are the mean upper-layer thicknesses for the northern and southern gyres, respectively. Equation (26) is not valid for models beyond QG, but (27) in terms of layer thicknesses might provide a useful quantification of the asymmetry induced by the wind forcing when applied to a primitive equation model. In the BB model (Fig. 1c), the average interface displacement in each gyre is of the order of 60 m and the displacement of the jet's separation latitude resulting from (27) is 200 km, which is approximately the observed difference in the jet's position between BB and SPEM (see Fig. 1). This analogy does not take into account inertial and dissipation effects.

A significant difference is observed in the location of the jet separation between numerical models with levels or layers as vertical coordinate, and it has been shown in this paper that the prescription of the boundary conditions at the surface (wind forcing applied as a body force at the first level or over the upper layer) and at the walls (zero vorticity for free-slip condition) produce the different responses in the models. Because of the limited number of experiments at our disposal, it is difficult to quantify the importance of each boundary condition. Based on the results of section 3, the jet's position is strongly dependent on inertia, and the influence of the wind-forcing formulation will vary accordingly. As inertia decreases, the boundary condition at the walls becomes more important in influencing the separation. For the experiments presented in Fig. 1, both the wind-forcing formulation and the definition of the lateral boundary condition at the walls appear to be important in contributing to the observed differences in location of the midlatitude jet separation.

In the ocean, the depth over which the wind acts is time and space dependent and is usually assumed to be the depth of the mixed layer. In reality, the mixed layer is deeper in the subpolar gyre than in the subtropical gyre and neither level nor layer models capture this distribution. Therefore, one needs to include mixed-layer dynamics in a model to overcome the limitations of the simple body force assumption. On the other hand, the boundary-layer inconsistency illustrated in this paper can more easily be overcome in the implementation of numerical models.

Acknowledgments. J. McWilliams gave valuable assistance with interpretation of the results and numerical model formulation. EPC also thanks K. Haines for stimulating discussions. Conversations with R. Bleck, B. Cushman-Roisin, D. Haidvogel, and C. Rooth were timely and valuable. Many thanks to D. Haidvogel for providing the SPEM datasets. N. Norton built the QG and LBE models used in this study and helped analyze the results. The computations were carried out using the CRAYs at the National Center for Atmospheric Research (NCAR). NCAR is sponsored by the National Science Foundation.

REFERENCES

Bleck, R., and D. B. Boudra, 1981: Initial testing of a numerical ocean circulation model using a hybrid (quasi-isopycnic) vertical coordinate. *J. Phys. Oceanogr.*, **11**, 755–770.

——, and ——, 1986: Wind-driven spin up in eddy-resolving ocean models formulated in isopycnic and isobaric coordinates. *J. Geophys. Res.*, **91**, 7611–7621.

Haidvogel, D. B., J. L. Wilkin and R. Young, 1991: A semi-spectral primitive equation ocean circulation model using vertical sigma and orthogonal curvilinear horizontal coordinates. *J. Comput. Phys.*, **94**, 151–185.

Holland, W. R., 1978: The role of mesoscale eddies in the general circulation of the ocean—numerical experiments using a wind-driven quasi-geostrophic model. *J. Phys. Oceanogr.*, **8**, 363–392.

——, and L. B. Lin, 1975: On the generation of mesoscale eddies and their contribution to the oceanic general circulation. Part I: A preliminary numerical experiment. *J. Phys. Oceanogr.*, **5**, 642–657.

Huang, R. X., 1986: Numerical simulation of wind-driven circulation in a subtropical/subpolar basin. *J. Phys. Oceanogr.*, **16**, 1636–1650.

——, and G. Flierl, 1987: Two-layer models for the thermocline and current structure in subtropical/subpolar gyres. *J. Phys. Oceanogr.*, **17**, 872–884.

Lorenz, E. N., 1960: Energy and numerical weather prediction. *Tellus*, **12**, 364–373.

McWilliams, J. C., N. J. Norton, P. R. Gent and D. B. Haidvogel, 1990: A linear balance model of wind-driven, midlatitude ocean circulation. *J. Phys. Oceanogr.*, **20**, 1349–1378.

Moro, B., 1988: On the nonlinear Munk model. Part I: Steady flows. *Dyn. Atmos. Oceans*, **12**, 259–287.

Parsons, A. T., 1969: A two-layer model of Gulf Stream separation. *J. Fluid Mech.*, **39**, 511–528.

Pedlosky, J., 1979: *Geophysical Fluid Dynamics.* Springer-Verlag, 624 pp.

Thompson, J. D., and W. J. Schmitz, 1989: A limited-area model of the Gulf Stream: Design, initial experiments, and model-data intercomparison. *J. Phys. Oceanogr.*, **19**, 791–814.

Verron, J., and C. Le Provost, 1989: Asymmetrical wind forcing driving some numerical eddy-resolving general circulation experiments. *Mesoscale/Synoptic Coherent Structures in Geophysical Turbulence.* J. Nihoul and B. Jamart, Eds. Elsevier Oceanography Series, 407–433.

Welander, P., 1966: A two-layer frictional model of wind-driven motion in a rectangular oceanic basin. *Tellus*, **18**, 54–62.